

# Electron Spin Resonance of Ni-doped $\text{CuGeO}_3$ in the paramagnetic, spin-Peierls and antiferromagnetic states: Comparison with non-magnetic impurities

B. Grenier

*Département de Recherche Fondamentale sur la Matière Condensée, SPSMS-MDN, CEA/Grenoble, 17 rue des Martyrs, 38054 Grenoble, France*

*and Université Joseph Fourier Grenoble I, France*

P. Monod

*Laboratoire de Physique du Solide, Ecole Supérieure de Physique et Chimie, 10 rue Vauquelin, 75231 Paris, France*

M. Hagiwara, M. Matsuda\* and K. Katsumata\*\*

*RIKEN (The Institute of Physical and Chemical Research), Wako, Saitama 351-0198, Japan*

S. Clément and J.-P. Renard

*Institut d'Electronique Fondamentale, Bât.220, Université Paris-Sud, 91405 Orsay, France*

A.L. Barra

*Laboratoire des Champs Magnétiques Intenses, CNRS/MPG, 24 rue des Martyrs, 38042 Grenoble, France*

G. Dhalenne and A. Revcolevschi

*Laboratoire de Physico-Chimie de l'Etat Solide, Bât. 414, Université Paris-Sud, 91405 Orsay, France*

(November 19, 2018)

We have performed Electron Spin Resonance measurements on single crystals of the doped spin-Peierls compounds  $\text{CuGe}_{1-y}\text{Si}_y\text{O}_3$  and  $\text{Cu}_{1-x}\text{M}_x\text{GeO}_3$  with  $\text{M} = \text{Zn, Mg, Ni}$  ( $x, y \leq 0.1$ ). The first part of our experiments was performed in the paramagnetic and spin-Peierls phases at 9.5, 95 and 190 GHz. All non-magnetic impurities (Si, Zn and Mg) were found to hardly affect the position and linewidth of the single line resonance, in spite of the moment formation due to the broken chains. In contrast to Si, Zn and Mg-doping, the presence of Ni ( $S = 1$ ) at low concentration induces a spectacular shift towards high fields of the ESR line (up to 40% for  $x=0.002$ ), together with a large broadening. This shift is strictly proportional to the ratio of Ni to Cu susceptibilities: Hence it is strongly enhanced below the spin-Peierls transition. We interpret this shift and the broadening as due to the exchange field induced by the Ni ions onto the strongly exchange coupled Cu spins. Second, the antiferromagnetic resonance was investigated in Ni-doped samples. The frequency vs magnetic field relation of the resonance is well explained by the classical theory with orthorhombic anisotropy, with  $g$  values remarkably reduced, in accordance with the study of the spin-Peierls and paramagnetic phases. The easy, second-easy, and hard axes are found to be  $a$ ,  $c$ , and  $b$  axes, respectively. These results, which are dominated by the single ion anisotropy of  $\text{Ni}^{2+}$ , are discussed in comparison with those in the Zn- and Si-doped  $\text{CuGeO}_3$ .

## I. INTRODUCTION

The quasi-one dimensional compound  $\text{CuGeO}_3$  is the first inorganic system exhibiting a spin-Peierls (SP) transition<sup>1</sup>. It has been extensively studied since large single crystals are available, which allows to perform various kinds of experiments. The magnetic structure of  $\text{CuGeO}_3$  is as follows: the spin correlations are antiferromagnetic along the  $b$  and  $c$  axes and ferromagnetic along the  $a$ -axis. Below  $T_{SP} \simeq 14.3$  K, the  $S = \frac{1}{2}$  Heisenberg antiferromagnetic (AF) chains, running along the  $c$ -axis, become dimerized and an energy gap  $\Delta = 2$  meV opens between the singlet ground state and the first excited triplet states. The SP transition is evidenced by a kink at  $T_{SP}$  in the magnetic susceptibility

and is clearly revealed by X-ray and neutron scattering<sup>2</sup>. A unique feature of this compound is that the effect of impurities can be studied by substituting impurity ions (Zn, Mg and Ni) for the Cu sites<sup>3-8</sup> and Si for the Ge sites<sup>9</sup>. These substitutions all induce a strong decrease of  $T_{SP}$  and the appearance at lower temperature ( $T < T_N < T_{SP}$ ) of a three-dimensional AF phase. The most intriguing feature in the impurity effects is the coexistence below  $T_N$  of the SP state and the long-range AF ordering, which was extensively studied both experimentally<sup>10,11</sup> and theoretically<sup>12</sup>. Magnetization measurements performed in  $\text{Cu}_{1-x}\text{M}_x\text{GeO}_3$  (with  $\text{M} = \text{Zn, Mg, Ni}$ ) and  $\text{CuGe}_{1-y}\text{Si}_y\text{O}_3$  single crystals have revealed the existence of a universal Temperature - Doping concentration phase diagram with a scaling factor

$x = 3y^{13}$ . The spin-Peierls temperature shows a linear decrease as the doping level increases, following the relation  $T_{SP}(x, y)/T_{SP}(0) = 1 - 15x = 1 - 44y$ , while the Néel temperature increases linearly from 0 at low doping levels up to a broad maximum around 4.5 K for  $x = 3y \simeq 0.04$  and then gradually decreases. Thus, doping on the Ge site by Si impurities (spin 0) is three times more efficient than doping on the Cu site, either by magnetic (Ni: spin 1) or non-magnetic (Zn, Mg) impurities. For all non-magnetic impurities, the easy axis in the AF phase is the  $c$ -axis<sup>6,9,10,13-17</sup>. However, some deviations from this universal behavior are noted in the case of Ni concerning the AF phase. Indeed, the  $T_N(x)$  curve for Ni is slightly lower<sup>13</sup> and the easy axis was found to be the  $a$ -axis from susceptibility<sup>13,18</sup> and neutron scattering experiments<sup>7</sup>.

Electron spin resonance (ESR) studies of the paramagnetic and spin-Peierls phases have been performed by different authors in pure<sup>19-22</sup>, Si-, and Zn-doped  $\text{CuGeO}_3$ <sup>16,23,24</sup>, and the antiferromagnetic resonance has also been studied for these two substitutions<sup>15-17</sup>. But very little has been done using the ESR technique in Ni-doped  $\text{CuGeO}_3$ , besides the work of Glazkov et al.<sup>25</sup> where a large number of parameters is needed for the interpretation.

The first aim of this paper is to make a comparative ESR study of  $\text{Cu}_{1-x}\text{M}_x\text{GeO}_3$  (with  $\text{M} = \text{Zn, Mg, Ni}$ ) and  $\text{CuGe}_{1-y}\text{Si}_y\text{O}_3$  compounds, to find out if the universal character of the Temperature-Concentration phase diagram holds also for ESR, especially when comparing non-magnetic and magnetic impurities. Extensive ESR measurements were performed in the paramagnetic and spin-Peierls phases on high quality single crystals, for various doping levels. The results obtained in the non-magnetic impurity doped compounds are briefly presented and those obtained in Ni-doped  $\text{CuGeO}_3$  are focused on. For the latter, our results on the ESR line shift are analyzed in detail and a model is proposed to explain the observed effect.

The second aim of this paper is to study the antiferromagnetic resonance (AFMR) in Ni-doped  $\text{CuGeO}_3$  samples, and to compare the results with those obtained in the case of non-magnetic impurities. ESR is indeed a crucial technique to study the magnetic anisotropy at a microscopic level. In both studies (ESR and AFMR), Ni substitution is shown to produce different effects on the spin resonance of  $\text{CuGeO}_3$ , as compared to the case of non-magnetic impurities.

## II. EXPERIMENTAL SET UP

The  $\text{CuGe}_{1-y}\text{Si}_y\text{O}_3$  ( $y = 0, 0.002, 0.007, 0.0085, 0.015, 0.06, 0.085$ ) and  $\text{Cu}_{1-x}\text{M}_x\text{GeO}_3$  ( $\text{M} = \text{Zn}$  with  $x = 0.016, 0.039, 0.01$ ;  $\text{M} = \text{Mg}$  with  $x = 0.01, 0.03, 0.05$ ;  $\text{M} = \text{Ni}$  with  $x = 0.002, 0.0085, 0.02, 0.03, 0.04$ ) single crystals used in this study were grown from the melt under

oxygen atmosphere using a floating zone method associated with an image furnace. All samples were then analyzed using Inductively Coupled Plasma Atomic Emission Spectroscopy (ICP/AES). The doping levels that are reported here are thus the effective ones derived from the ICP/AES analysis, which are usually slightly lower than the nominal concentration.

The ESR measurements were performed between 4 and 300 K in all single crystals on a standard X-band spectrometer (Bruker ESP 300E), operating at a frequency  $f \simeq 9.5$  GHz and in a field range  $\pm 1.6$  T. With this apparatus, the measured signal is the field derivative of the absorption. The crystal of typical mass 5 to 10 mg can be mounted onto the sample holder in order that the magnetic field lies either in the  $(a, b)$  or in the  $(a, c)$  plane. Because of the huge broadening of the ESR line induced by Ni-doping, further measurements were performed on a home-made high field spectrometer. These experiments were crucial to interpret the observed phenomena. The measurements were performed between 4 and 250 K at frequencies 95 and 190 GHz, with the field parallel to the  $c$ -axis. The sample size was about  $4 \times 8 \times 8$  mm<sup>3</sup>, corresponding to a mass of more than 500 mg. With this spectrometer, the measured ESR signal is the field derivative of a combination of the dispersion and absorption. The AFMR measurements were performed on two  $\text{Cu}_{1-x}\text{Ni}_x\text{GeO}_3$  single crystals, with  $x = 0.03$  and  $0.04$ , in the frequency ranges of 9, 20, 35, and 50 GHz and a temperature of 1.8 K (*i.e.* below  $T_N$ ). The dimension of the crystals used in these experiments is about  $3 \times 3 \times 2$  mm<sup>3</sup>. We used an X-band spectrometer (JOEL-JES-RE3X) for the experiments around 9 GHz and a home-made spectrometer for higher frequencies. For the latter, microwaves are generated from two klystrons at 20 and 50 GHz and from a Gunn-oscillator at 35 GHz, the magnetic field ( $B$ ) being produced by a 20 T superconducting magnet from Oxford Instruments. The magnetic susceptibility measurements in the Ni-doped samples are also presented in this paper (for the other compounds, see Ref. 13): they were performed on a home-made SQUID magnetometer operating in the temperature range 1.8 – 300 K and in the magnetic field range 0 – 8 T.

## III. ESR IN $\text{CuGeO}_3$ DOPED WITH NON-MAGNETIC IMPURITIES

The temperature dependence of the magnetic susceptibility was first measured in all the samples whose ESR study is presented here (see Ref. 26 for Si-doping and Ref. 13 for Si, Zn and Mg-doping). We present briefly in this section the ESR results obtained in the case of non-magnetic impurities and discuss the linewidth, the shift, and the integrated intensity of the resonance line.

A wide series of  $\text{CuGeO}_3$  samples doped with non-magnetic impurities Si, Zn, and Mg (see the list in sec. II) and a sample of pure  $\text{CuGeO}_3$  were investigated. In

all Si-, Zn- and Mg-doped  $\text{CuGeO}_3$  compounds, a single lorentzian derivative ESR line was observed at X-band between 5 and 300 K along the three crystallographic axes, as for pure  $\text{CuGeO}_3$ .

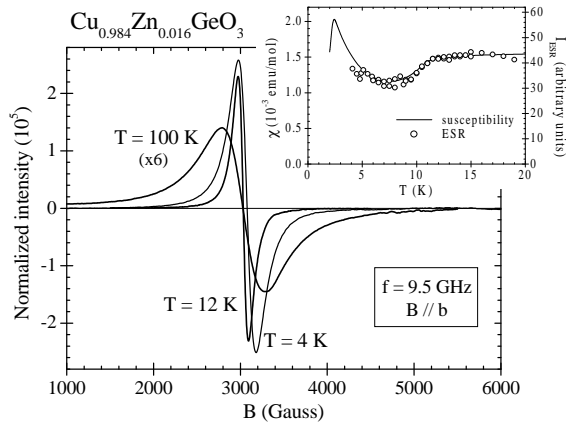


FIG. 1. ESR spectra obtained at X-band, with  $B \parallel b$ , in  $\text{Cu}_{0.984}\text{Zn}_{0.016}\text{GeO}_3$ , above and below the SP temperature. The inset illustrates the temperature dependence of the (twice) integrated ESR intensity as compared to that of the static susceptibility.

Figure 1 shows examples of spectra obtained in a 1.6% Zn-doped sample for  $B \parallel b$ , *i.e.* for the field perpendicular to the chain axis, and at different temperatures, above and below  $T_{SP} = 10.4$  K. In all these samples and along the three crystallographic directions, the linewidth  $\Delta B$  and its temperature dependence were found to be identical to those of pure  $\text{CuGeO}_3$  above 15 K<sup>27</sup>, but not below:  $\Delta B(T)$  depends on the Néel and SP temperatures, which vary with the doping level. As can be seen in Fig. 1, a 1% shift of the ESR line is observed only below  $T_{SP}$ . The same result was found in all  $\text{CuGeO}_3$  samples doped with non-magnetic impurities and also in the pure compound: The  $g$  values remain constant down to 10-15 K and become shifted at lower temperature by less than 2%. The sign of the shift depends on the field orientation and on the substituent, which agrees well with the results of Hase *et al.*<sup>23</sup> obtained on pure, Zn- and Si-doped  $\text{CuGeO}_3$ . For pure and Si-doped  $\text{CuGeO}_3$ , the  $g$ -factor is found to increase along  $b$  and to decrease along  $a$  and  $c$ , as temperature decreases. For Zn- and Mg-doped  $\text{CuGeO}_3$  the opposite behavior is observed for the three crystallographic directions.

The inset of Figure 1 shows the variation with temperature of the ESR (twice) integrated intensity  $I_{ESR}$  as compared to that of the static susceptibility, in the 1.6% Zn-doped  $\text{CuGeO}_3$  sample. Since both curves can be superimposed, we infer that ESR at X-band cannot distinguish between triplet spins (spin-Peierls contribution) and spins freed by impurities (Curie-Weiss contribution)<sup>13,26</sup>. We will come back to this point in Sec. V B. A similar investigation carried out on Zn-doped

$\text{CuGeO}_3$  (up to 5% Zn) on powder samples at high field (between 100 and 400 GHz) by Hassan *et al.*<sup>24</sup> yields results qualitatively different from the previous investigations at lower frequency (see Ref. 15,16 and present work). In Ref. 24, the appearance of two distinct powder pattern ESR spectra is interpreted as a separate contribution from the excited spin-Peierls triplet and the Zn-induced moments. Motivated by this apparent paradox, we have investigated the ESR in the paramagnetic phase of a single crystal of  $\text{CuGeO}_3$  : 5% Zn at 95 GHz and 5 K. Contrary to Ref. 24, we observe for all field directions in the (a, b) plane a single resonance line varying from  $g_a = 2.145$  to  $g_b = 2.240$ , in accordance with our X-band measurements. Thus, we are forced to conclude that the additional ESR powder pattern observed by Hassan *et al.*<sup>24</sup> is somehow linked to the powdered nature of the investigated samples.

#### IV. MAGNETIC SUSCEPTIBILITY IN Ni-DOPED $\text{CuGeO}_3$

Figure 2 shows the temperature dependence of the magnetic susceptibility measured in pure  $\text{CuGeO}_3$  and in  $\text{Cu}_{1-x}\text{Ni}_x\text{GeO}_3$  samples in the 1.8-300 K temperature range (Fig. 2b) and below 30 K (Fig. 2a).

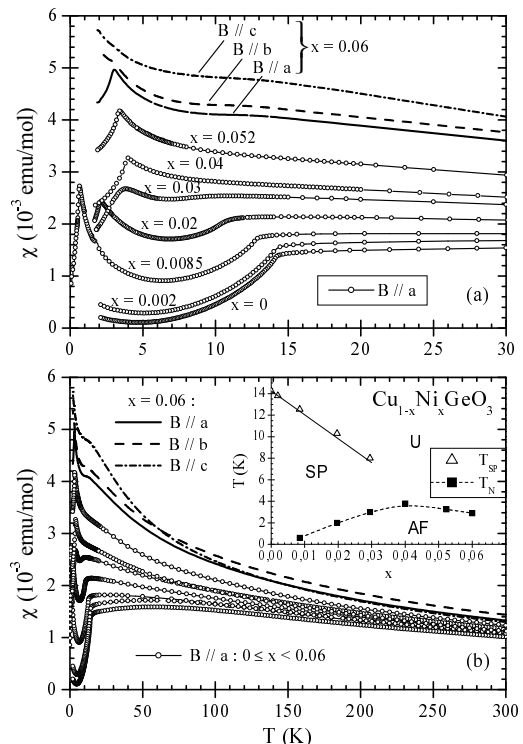


FIG. 2. Temperature dependence of the magnetic susceptibility measured in  $\text{Cu}_{1-x}\text{Ni}_x\text{GeO}_3$  samples in a 1 kGauss field applied along the  $a$ -axis (easy axis) for  $0 \leq x \leq 0.052$  and along the three crystallographic axes for  $x = 0.06$ . The inset of figure (b) displays the  $(T, x)$  phase diagram obtained from these measurements.

## A. Experimental results

The data from Figure 2a clearly show the decrease of the SP transition (which is visible up to  $x = 0.03$ ) and the occurrence of the AF transition at lower temperature, with  $a$  being the easy axis. Indeed, the susceptibility measured with the external field along the  $a$ -axis shows a peak, around 3 K for  $x = 0.06$  (see solid line), while the susceptibilities measured with the external field along the  $b$  and  $c$  axes further increase below 3 K with decreasing temperature (see dash and dash-dot lines). The  $\text{Ni}^{2+}$  ion, with  $S = 1$ , is considered to participate to the long-range magnetic ordering since the magnitude of the Curie tail is one order of magnitude smaller than expected from 6% Ni free spins, indicating that the interaction between the  $\text{Cu}^{2+}$  and  $\text{Ni}^{2+}$  ions is relatively large. The  $(T, x)$  phase diagram shown in the inset of Fig. 2b was obtained from these measurements. The values of the spin-Peierls and Néel temperatures (when they exist) are given in Table I. For  $x = 0.002$ , the susceptibility measurement was performed only down to  $T = 1.8$  K, so that the Néel temperature (expected to be smaller than the 0.6 K value obtained for  $x = 0.0085$ ) could not be determined.

Figure 2b illustrates the large effect of Ni-doping on the global susceptibility curve, due to the magnetic nature of the  $\text{Ni}^{2+}$  ion. Indeed, the susceptibility increases more and more between 300 and 20 K as the Ni concentration increases. Interestingly, the susceptibilities along the  $a$  and  $b$  axes become smaller than the one along  $c$  below  $\simeq 50$  K. This anomalous temperature dependence was not observed in Si- and Zn-doped  $\text{CuGeO}_3$ <sup>9,13,28</sup>. This could originate from the single ion anisotropy of  $\text{Ni}^{2+}$  ions  $DS_z^2$  with  $z$  along the direction of the distorted oxygen octahedron in the  $(a, b)$  plane, as clearly observed with  $\text{Mn}^{2+}$  (Ref. 29). This will be further discussed in the AFMR results presented in Sec. VI.

The temperature dependence of the susceptibility could be analyzed in the paramagnetic phase ( $T > 20$  K) by a crude model of Cu-Ni pairs, neglecting in a first step the single ion anisotropy of  $\text{Ni}^{2+}$ , yielding an estimate of the Ni-Cu antiferromagnetic exchange coupling of 25 K<sup>13</sup>. This value is to be compared to the strongest Cu-Cu coupling,  $J_c = 120 - 180$  K along the  $c$ -axis. The susceptibility data from Figure 2 will be used later on to explain the ESR results.

TABLE I. Spin-Peierls and Néel temperatures (when they exist) for the pure and Ni-doped  $\text{CuGeO}_3$  samples.

$x$	$T_{SP}$ (K)	$T_N$ (K)
0	14.25	—
0.002	13.8	< 1.8
0.0085	12.55	0.6
0.02	10.3	2
0.03	8	3
0.04	—	3.8
0.052	—	3.25
0.06	—	2.9

The Ni-doped  $\text{CuGeO}_3$  samples were investigated at X-band along the three crystallographic directions and at high frequency along the  $c$ -axis. Figure 3 shows typical ESR spectra obtained in  $\text{Cu}_{0.998}\text{Ni}_{0.002}\text{GeO}_3$  ( $T_{SP} = 13.8$  K) at X-band along the  $c$ -axis at  $T = 100, 12$  and 4 K. Figure 4 shows ESR spectra obtained in  $\text{Cu}_{0.9915}\text{Ni}_{0.0085}\text{GeO}_3$  ( $T_{SP} = 12.55$  K) at 95 GHz along the  $c$ -axis at  $T = 100, 11$  and 7 K. In all Ni-doped compounds, a single lorentzian derivative ESR line was again observed but its linewidth  $\Delta B$  and resonance field  $B_{res}$  behave in a completely different way. Qualitatively, as compared to Fig. 1 for 1.6% Zn-doping, one notices immediately on Fig. 3 for 0.2% Ni-doping (X-band) and Fig. 4 for 0.85% (95 GHz) that a  $\sim 5\%$  shift towards high field is already visible in the spectra at 12 and 11 K respectively, compared to those at 100 K. This shift increases to reach 24% at 7 K (Fig. 4) and 36% at 4 K (Fig. 3) which is much larger than the  $\sim 1\%$  shift measured in Fig. 1. Moreover, one notes the large broadening induced by Ni-doping: the spectrum measured at 100 K for 0.2% Ni-doping (see Fig. 3) is about three times broader than for 1.6% Zn-doping (see Fig. 1) or pure  $\text{CuGeO}_3$ . This large broadening justifies the use of higher frequencies for further studies of the Ni-doped  $\text{CuGeO}_3$  samples.

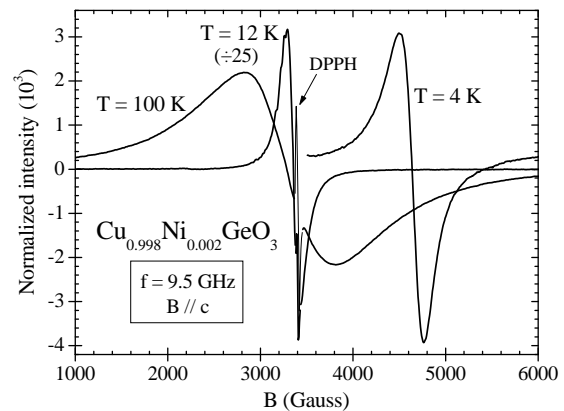


FIG. 3. ESR spectra obtained in X-band, with  $B \parallel c$ , in  $\text{Cu}_{0.998}\text{Ni}_{0.002}\text{GeO}_3$ , above and below the SP temperature. The figure shows the huge broadening of the ESR line on each side of  $T_{SP}$  and the increasing shift towards high fields as  $T$  decreases.

The spectra obtained in X-band ( $f = 9.5$  GHz) correspond to the field derivative of the absorption  $\chi''$  while those obtained in the millimetric domain ( $f = 95$  and 190 GHz) correspond to the field derivative of a combination of the absorption  $\chi''$  and dispersion  $\chi'$ . In order to check the lorentzian profile and to extract precisely the integrated intensity (meaningfull at X band only), the linewidth, and the resonance field for each measured

spectrum, the data obtained in the X and millimetric domains were fitted to the relation:

$$S(B) = S_0(B) + \frac{d\chi''}{dB} \cos \alpha + \frac{d\chi'}{dB} \sin \alpha \quad (1)$$

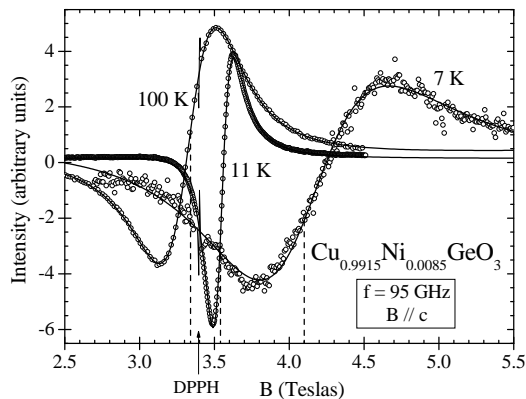


FIG. 4. ESR spectra obtained at 95 GHz, with  $B \parallel c$ , in  $\text{Cu}_{0.9915}\text{Ni}_{0.0085}\text{GeO}_3$ , above and below the SP temperature. Note the large broadening on each side of  $T_{SP}$  and the increasing shift towards high fields as  $T$  decreases. The solid lines are the best Lorentzian fits to the experimental data (see Eq. (1)), and the dash lines point out the position of the resonance field at each temperature, obtained from the fit.

where  $S_0(B)$  is a linear function in  $B$  accounting for the base line,  $\alpha$  is the phase (equal to zero at X band),  $\chi''(B)$  and  $\chi'(B)$  are Lorentzian shape centered at the resonance field  $B_{res}$ , with an integrated intensity  $I_{ESR}$  and a Lorentzian linewidth  $\Delta B^{Lorentz}$ . The "peak to peak" linewidth  $\Delta B$  of the ESR spectra is given by  $\Delta B = \frac{\sqrt{3}}{2} \Delta B^{Lorentz}$ . Figure 4 illustrates the very good quality of the fits to Eq. (1) of a few ESR spectra measured in  $\text{Cu}_{0.9915}\text{Ni}_{0.0085}\text{GeO}_3$  at 95 GHz for three different temperatures. Typical precisions are less than 1% on the determination of  $\Delta B$  and less than 0.01% for  $B_{res}$ , the precision on the phase  $\alpha$  (in the case of the millimetric range) being always better than  $1^\circ$ .

### 1. Integrated intensity at X band

In the case of X band, the ESR integrated intensity can be compared to the static susceptibility measured with the SQUID magnetometer. ESR spectra were measured in three  $\text{Cu}_{1-x}\text{Ni}_x\text{GeO}_3$  samples. For  $x = 0.002$ , the ESR line could be followed between 4 and 300 K, but due to the very large broadening induced by Ni-doping, the ESR line could be followed only up to 30 K for  $x = 0.0085$  and up to 20 K for  $x = 0.02$ . All spectra measured for  $x = 0.002$  were analyzed using Eq. (1) with  $\alpha = 0$  and  $S_0(B) = 0$  and the ESR (twice) integrated intensity  $I_{ESR}$  was obtained for each temperature. Due to the strong lineshift induced by Ni-doping, the resonance field must be taken into account and the static susceptibility

measured by SQUID has thus to be compared with the following ratio:

$$I'_{ESR} = I_{ESR} \left( \frac{B_0}{B_{res}} \right) \quad (2)$$

where  $B_0$  is the resonance field of pure  $\text{CuGeO}_3$  measured at the same frequency and along the same direction (*i.e.* corresponding to  $g_c = 2.05$  in the present case where  $B \parallel c$ ). Note that in the case of non-magnetic impurities, the static susceptibility was directly compared to  $I_{ESR}$  since the resonance field varied by less than 2% on the whole temperature range.

Figure 5 displays the temperature dependence of  $I'_{ESR}$  (right scale) compared to the macroscopic susceptibility vs temperature  $\chi(T)$  in the same sample ( $x = 0.002$ ) and in pure  $\text{CuGeO}_3$  (left scale), in a logarithmic scale. The SQUID measurements were performed in a 0.1 T magnetic field applied along the  $c$ -axis while the ESR measurements were performed in a sweeping field from 0 to 6600 G applied along the same axis. By adjusting the  $\chi(T)$  and  $I'_{ESR}(T)$  curves at high temperature, one can note that the ESR integrated intensity follows better the susceptibility of the pure sample than that of the 0.2% Ni-doped sample. This results leads one to suggest that the ESR signal would originate only from the  $\text{Cu}^{2+}$  spins of  $\text{CuGeO}_3$  while the  $\text{Ni}^{2+}$  spins would not participate to this resonance line<sup>30</sup>.

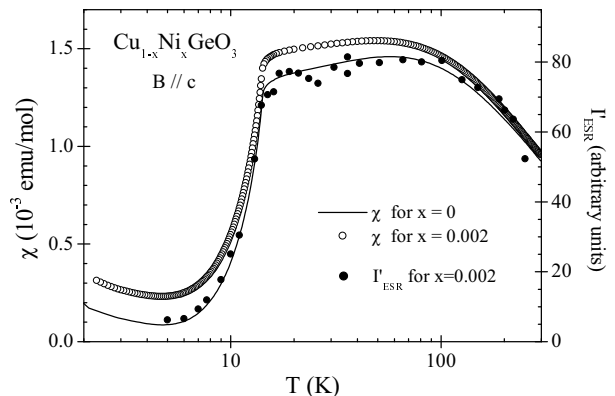


FIG. 5. Temperature dependence of the static susceptibility (SQUID) measured with  $B = 0.1 \text{ T} \parallel c$  in pure and 0.2% Ni-doped  $\text{CuGeO}_3$  (left scale) compared to the susceptibility derived from the ESR measurements ( $I'_{ESR} = I_{ESR} \cdot B_0 / B_{res}$ ) in the same Ni-doped sample and with  $B \parallel c$  (right scale), on a logarithmic T scale.  $I'_{ESR}(T)$  fits better with the static susceptibility of pure  $\text{CuGeO}_3$ .

To check this assumption, the same comparison was performed for a higher Ni-doped sample ( $x = 0.02$ ). Here again, the static susceptibility vs temperature curves of  $\text{Cu}_{0.98}\text{Ni}_{0.02}\text{GeO}_3$  and pure  $\text{CuGeO}_3$  are compared with the  $I'_{ESR}(T)$  curve derived from the ESR measurements in the same Ni-doped sample. For an easier comparison, the susceptibility data were normalized at 20 K (by dividing for each temperature  $\chi(T)$  by  $\chi(T = 20 \text{ K}) = \chi_{20}$ )

and all the curves are plotted as a function of the reduced temperature  $T/T_{SP}$ , with  $T_{SP} = 14.25$  K for  $x = 0$  and  $T_{SP} = 10.3$  K for  $x = 0.02$  (see Fig. 6). Indeed, for such a high Ni-doping level, the spin-Peierls temperatures and the absolute value of the static susceptibility are quite different from the pure sample (see Fig. 2a). By normalizing the susceptibility and ESR data at 20 K, one can notice that the  $I'_{ESR}$  curve lies in between the normalized susceptibilities of pure and Ni-doped  $\text{CuGeO}_3$ .

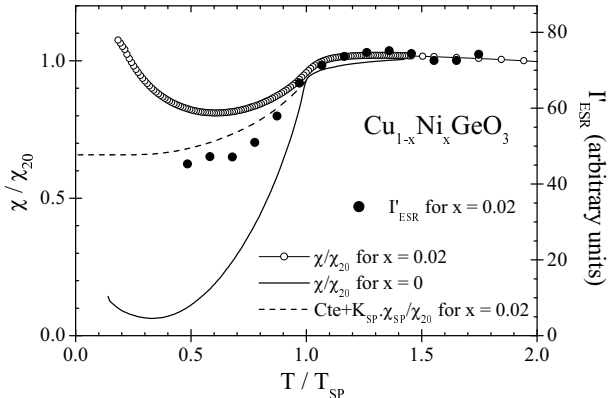


FIG. 6. Static susceptibility (SQUID) measured with  $B = 0.1$  T  $\parallel c$  in pure ( $T_{SP} = 14.25$  K) and 2% Ni-doped  $\text{CuGeO}_3$  ( $T_{SP} = 10.3$  K), normalized at 20 K (left scale), compared to the susceptibility derived from the ESR measurements ( $I'_{ESR}$ ) in the same Ni-doped sample and with  $B \parallel c$  (right scale), as a function of the reduced temperature  $T/T_{SP}$ . The dash line (left scale) represents the SP contribution to the global susceptibility of 2% Ni-doped  $\text{CuGeO}_3$  arising from the model described in Ref. 13 (see text).

Since it was shown<sup>13,26</sup> that the amplitude of the SP order parameter (expressed by the fraction  $K_{SP}$ ) is reduced in presence of doping (by Ni, Zn, Mg, Si), we have analyzed our data accordingly. In particular, for  $\text{Cu}_{1-x}\text{Ni}_x\text{GeO}_3$  with  $x = 0.02$ ,  $K_{SP}$  was found to be equal to 0.465<sup>13</sup>, *i.e.* only approximately one half of the Cu spins are able to dimerize so that the decrease of  $\chi(T)$  is much smaller than for pure  $\text{CuGeO}_3$ . Moreover, the decrease of the energy gap upon doping further amplifies this effect. Thus, our ESR intensity data have to be compared with this (reduced) SP contribution instead of that of the full susceptibility of pure  $\text{CuGeO}_3$ . The dash line from Fig. 6 shows the temperature dependence of this SP contribution (divided by the  $\text{Cu}_{0.98}\text{Ni}_{0.02}\text{GeO}_3$  susceptibility at 20 K) normalized at  $T/T_{SP} = 1$  with the curve of the pure sample. One can note the good agreement between this curve and the  $I'_{ESR}$  data. This analysis further supports the idea that the ESR signal only comes from the  $\text{Cu}^{2+}$  spins. We will come back to these results when discussing the lineshift results (see Sec. VB). The same study has been performed for a magnetic field applied along the  $a$ -axis and the results were found to be similar.

## 2. Linewidth

Besides the large ESR shift, the other main qualitative effect of Ni-doping is a very large broadening of the ESR line as compared to pure  $\text{CuGeO}_3$ . This is further contrasted by the linewidth data of  $\text{CuGeO}_3$  doped by the non-magnetic impurities Zn, Mg or Si<sup>27</sup>. In Fig. 7a, the low temperature linewidth data are presented at X band for pure  $\text{CuGeO}_3$  and various Ni-doping levels. It appears that above  $T_{SP}$  and up to about 40 K, the linewidth increases linearly with temperature and is approximately proportional to the Ni concentration at a rate of  $\Delta B/x \sim 1000$  G/%Ni for  $T = 20$  K and a slope  $\Delta B/(x.T) \sim 100$  G.K<sup>-1</sup>/%Ni.

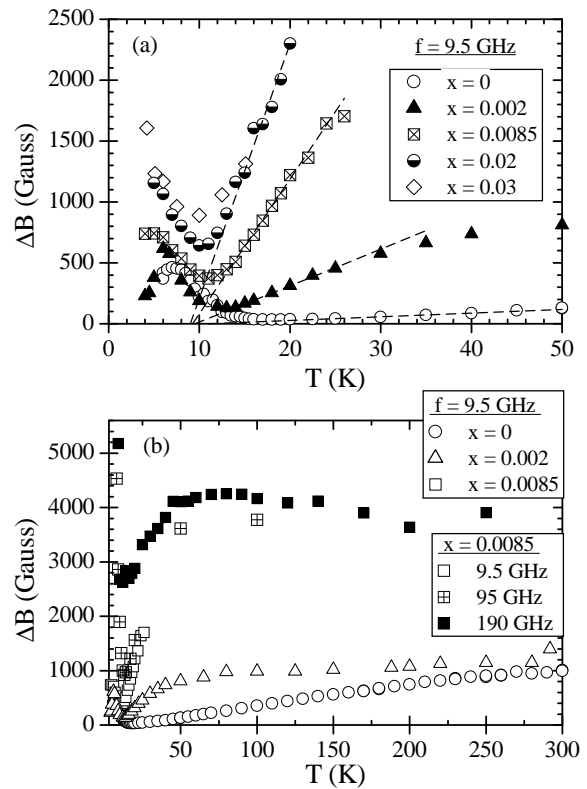


FIG. 7. Temperature dependence of the ESR linewidth measured with  $B \parallel c$  in pure and Ni-doped  $\text{CuGeO}_3$  for various concentrations: a) Low temperature part at X band; b) High temperature part at X band and higher frequencies. Note the plateau above 50 K for 0.2 and 0.85% Ni.

However, as shown in Fig. 7b, contrary to the pure  $\text{CuGeO}_3$  linewidth data, where the linear temperature dependence extends almost up to room temperature (see also Ref. 19,20), the Ni-doped  $\text{CuGeO}_3$  ESR linewidth reaches a plateau above 50 K independent of both the temperature and the magnetic field. This plateau is proportional to the Ni concentration at a rate  $\Delta B_{\text{plateau}}/x \simeq 4600$  G/%Ni. At temperatures lower than  $T_{SP}$ , a temperature behavior much closer to that of pure  $\text{CuGeO}_3$  is observed with a comparable rate of broadening (see Fig.

7a), but now strongly increasing with field (see Fig. 7b). Whereas we cannot account at present for the temperature dependence of the linewidth, the order of magnitude of  $\Delta B_{\text{plateau}}$  is discussed in Sec. VB.

### 3. Lineshift along the $c$ -axis

We now focus on the ESR lineshift  $\delta B = B_{\text{res}} - B_0$ , measured for  $B \parallel c$ ,  $B_{\text{res}}$  being the resonance field of the studied sample and  $B_0$  the resonance field of pure  $\text{CuGeO}_3$  (corresponding to  $g_c = 2.05$ ) measured at the same frequency. The aim of the following analysis is to study the field (or frequency), concentration and temperature dependence of the shift in order to derive experimentally an expression of  $\delta B(f, x, T)$ .

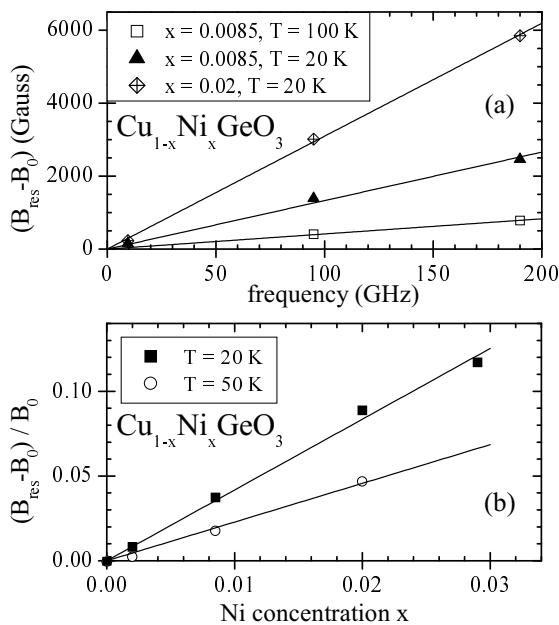


FIG. 8. (a) Frequency dependence of the ESR lineshift  $\delta B = B_{\text{res}} - B_0$  measured in  $\text{Cu}_{1-x}\text{Ni}_x\text{GeO}_3$  at two given temperatures. (b) Evolution with the nickel concentration of the relative lineshift measured at two different temperatures in four  $\text{Cu}_{1-x}\text{Ni}_x\text{GeO}_3$  single crystals. These two figures establish the proportionality (a) between the lineshift and the frequency at given temperature and Ni concentration, and (b) between the relative shift and the Ni concentration, at a given temperature (see solid lines).

Figure 8a shows the frequency dependence of the lineshift measured for two different samples, 0.85 and 2% Ni-doped  $\text{CuGeO}_3$ , and two different temperatures. This figure shows that the shift is proportional to the working frequency (see solid lines) and thus to  $B_0$ , which proves that it is a genuine "g-shift". This shift increases with  $x$  and  $T^{-1}$ . To study the concentration and temperature dependences, we will thus now refer to the frequency-independent relative shift  $\delta B/B_0$ . Figure 8b shows the

Ni concentration dependence of  $\delta B/B_0$  at two given temperatures,  $T = 20$  and  $50$  K (data from various frequencies were combined together to obtain this figure). For both temperatures, the relative shift is proportional to the Ni concentration, up to 3% (see solid lines). At this stage, we thus have the relation:

$$\frac{\delta B}{B_0}(x, T) = C(T) \cdot x \quad (3)$$

All our experimental results about the lineshift are gathered in Figure 9 using the above relation, *i.e.* the relative lineshift normalized to the Ni concentration  $\delta B/(100x \cdot B_0)$  is plotted as a function of the reduced temperature  $T/T_{\text{SP}}(x)$ . This figure shows the good agreement of relation (3) with our data. All the experimental points are roughly on a unique curve  $C(T)$ , at least above  $T_{\text{SP}}$ . Below the spin-Peierls temperature, the temperature dependence of  $\delta B/B_0$  depends on the Ni-doping level. Indeed, the data at 9.5 and 95 GHz are well superimposed down to  $0.7 T_{\text{SP}}$  for both samples with  $x = 0.0085$  and  $x = 0.02$ , but the increase at lower temperature is stronger as the Ni concentration decreases (see inset of Fig. 9).

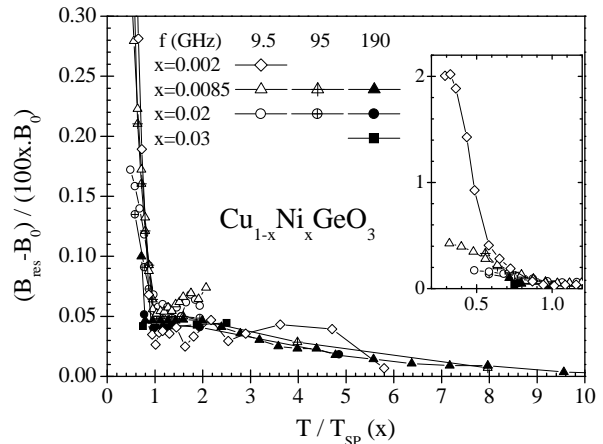


FIG. 9. Relative lineshift  $\delta B/B_0$  normalized by the Ni concentration (divided by  $100x$ ) as a function of the reduced temperature  $T/T_{\text{SP}}(x)$  for all studied Ni-doped  $\text{CuGeO}_3$  samples (various concentrations at various frequencies). The inset shows the low temperature part.

Thus, in order to study in detail the temperature dependence of the shift, we consider separately the paramagnetic (P) and SP phases. The temperature dependence of the relative shift in the 0.85% Ni-doped sample is illustrated for two different frequencies in Figures 10a for  $T > T_{\text{SP}}$  and 11a for  $T < T_{\text{SP}}$ . Between 300 and 20 K,  $\delta B/B_0$  increases up to 4% (see Fig. 10a) and its temperature dependence behaves like the nickel susceptibility  $\chi_{\text{Ni}}(T)$  (see Fig. 10b). The latter has been derived by subtracting the susceptibility of pure  $\text{CuGeO}_3$  to that of the Ni-doped sample (both presented in Fig. 1b). The

inset of Figure 10b shows that  $\delta B(T)/B_0$  is strictly proportional to  $\chi_{Ni}(T)$  in the P phase.

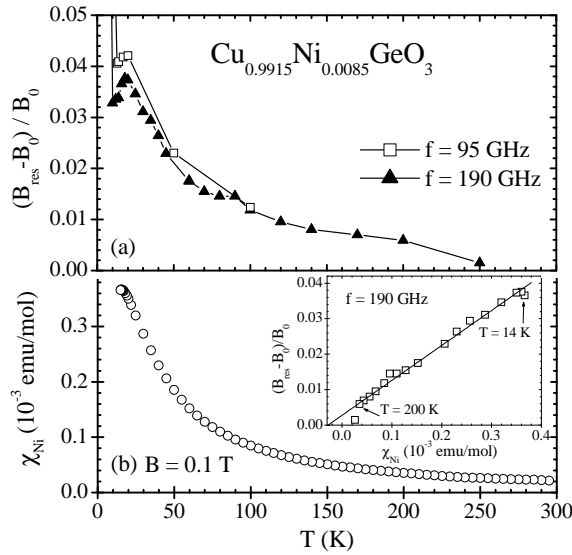


FIG. 10. Temperature dependence in the paramagnetic phase of (a) the relative ESR lineshift and (b) the static susceptibility of the Ni ions, measured in  $\text{Cu}_{0.9915}\text{Ni}_{0.0085}\text{GeO}_3$ . The inset of Fig. 10b illustrates the relative ESR lineshift as a function of the Ni susceptibility, at each temperature.

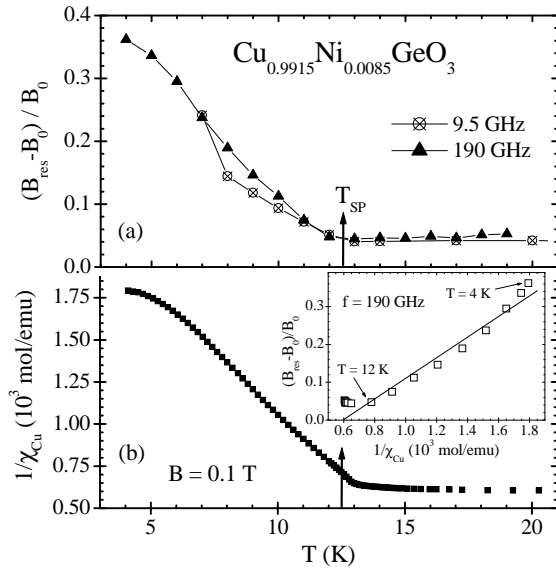


FIG. 11. Temperature dependence in the spin-Peierls phase of (a) the relative ESR lineshift and (b) the inverse static susceptibility of the Cu dimers, measured in  $\text{Cu}_{0.9915}\text{Ni}_{0.0085}\text{GeO}_3$ . The inset of Fig. 11b illustrates the relative ESR lineshift as a function of the inverse Cu susceptibility, at each temperature.

Concerning the low temperature part, one can notice a strong enhancement of the line shift below 12.5

K at 9.5 and 190 GHz (see Fig. 11a). This temperature corresponds to the SP transition, thus this behavior is mainly related to the dimerization of the Cu ions into  $S = 0$  states. Figure 11b illustrates the temperature dependence of the inverse of the Cu-dimers susceptibility (spin-Peierls contribution in the triplet state  $S = 1$ )  $\chi_{Cu}(T)$ , which was obtained by subtracting a Curie-Weiss contribution (coming from the Ni ions) to the total susceptibility<sup>13</sup>. As can be seen in the inset of Figure 11b,  $\delta B(T)/B_0(T)$  varies linearly with  $1/\chi_{Cu}(T)$ . This analysis of the data leads to the following relation for the relative shift:

$$\frac{\delta B}{B_0}(x, T) \propto x \cdot \frac{\chi_{Ni}(T)}{\chi_{Cu}(T)} \quad (4)$$

For the same reason as for the integrated intensities (decrease of the fraction  $K_{SP}$  when  $x$  increases), this formula is indeed consistent with the inset of Fig. 9 where the relative shift below  $T_{SP}$  shows a fourfold increase as the Ni doping level decreases from 0.85% to 0.2%.

#### 4. Anisotropy of the lineshift

The anisotropy of the lineshift has also been carefully studied at X-band in the 0.2% Ni-doped compound at 4 K, in the  $(a, c)$  and  $(a, b)$  planes (see Fig. 12).

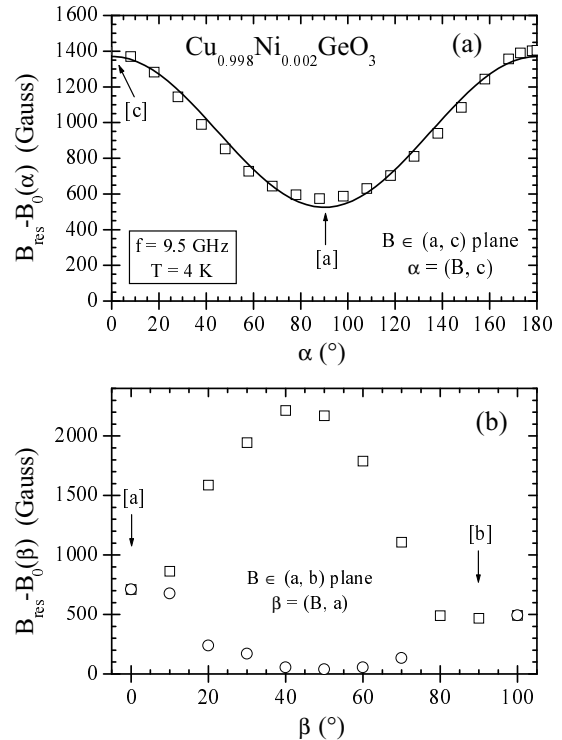


FIG. 12. Anisotropy of the ESR lineshift in the  $(a, c)$  and  $(a, b)$  planes measured in X-band, at  $T = 4$  K in 0.2% Ni-doped  $\text{CuGeO}_3$ . The open squares correspond to the aforementioned ESR line and the open circles to the new line that appears in the  $(a, b)$  plane.

The shift  $\delta B$  was found to be very anisotropic in both planes and a second, less intense, resonance line was observed in the  $(a, b)$  plane. In the  $(a, c)$  plane, the shift is maximum along  $c$  ( $\simeq 1400$  Gauss) and minimum along  $b$  ( $\simeq 600$  Gauss), following  $\delta B(\alpha) = \delta B_{ac} + \delta B_{anis} \cos \alpha$  with  $\delta B_{ac} \simeq 950$  and  $\delta B_{anis} \simeq 420$  Gauss. In the  $(a, b)$  plane, the shift is minimum and equivalent along the  $a$  and  $b$  axes while a maximum shift (2200 Gauss) is found at  $\beta \simeq 45^\circ$  (where  $\beta$  is the angle between the applied magnetic field and the  $a$ -axis) possibly reflecting the anisotropy of the Cu to the Ni site coupling. Note that the anisotropy of the lineshift along the crystal axes follows that of the static susceptibility (see Fig. 2b for the 6% Ni-doped CuGeO<sub>3</sub> sample).

## B. Resonance Model

The model used to interpret the ESR data of CuGeO<sub>3</sub> doped with Ni at very low concentrations is constrained by the above mentioned experimental observations which we briefly recall:

i- At all temperatures, along the  $a$ ,  $b$ , and  $c$  directions, only one Lorentzian shaped (except at the lowest temperature) ESR line is observed, above and below the spin-Peierls transition, which we attribute to the paramagnetic Cu<sup>2+</sup> spins above  $T_{SP}$  and to the excited triplet Cu<sup>2+</sup> spins below  $T_{SP}$ .

ii- No resonance consistent with Ni<sup>2+</sup> in a distorted octahedral site is observed in the temperature range  $4 < T < 300$  K, neither at 9.5 GHz nor up to 190 GHz and 10 Tesla.

iii- The ESR integrated intensity, normalized to the resonance field, does not scale with the static susceptibility measured in the same Ni-doped sample, but only to the proportion of Cu spins being in the SP triplet state, which supports i-.

iv- The width of the Cu<sup>2+</sup> resonance strongly increases with the Ni concentration (at a rate of 0.1 Tesla/% Ni at 20 K).

v- A resonance shift of the Cu<sup>2+</sup> line towards higher fields, proportional to the concentration of the Ni<sup>2+</sup> ions, is observed, above and below the spin-Peierls transition. This shift is proportional to the Ni ions susceptibility and inversely proportional to the Cu ions susceptibility. This shift thus becomes particularly noticeable below the SP transition. The shift is anisotropic, being roughly twice as large for the  $c$ -direction as for the  $a$  and  $b$  directions, which are about equivalent: it appears then that this shift is not related to the  $g$ -factor anisotropy of the pure CuGeO<sub>3</sub> system ( $g_a = 2.15$ ,  $g_b = 2.26$ ,  $g_c = 2.05$ ).

A very detailed investigation of a two coupled paramagnetic spins system, present in RbMnF<sub>3</sub> doped with Ni, Co or Fe, has been performed by Gulley and Jaccarino<sup>31</sup>. For 1 to 5% Ni-doping, contrary to the present work, no discernable linewidth broadening together with a small  $g$ -shift of 0.5% are observed. This situation was quan-

titatively analyzed in terms of very strongly exchange-coupled Ni and Mn spins. This is clearly not the case for CuGeO<sub>3</sub> : Ni but does apply to the case of CuGeO<sub>3</sub> : Zn, Mg or Si. Indeed, in addition to the absence of broadening and to the 1%  $g$ -shift, the fact that the ESR integrated intensity fits well the static susceptibility constitutes a compelling evidence for the strong coupling between the bulk Cu<sup>2+</sup> spins and the Cu<sup>2+</sup> spins induced by the non magnetic impurities.

The model used for our interpretation is an extension of Kittel's analysis for the ferrimagnetic resonance shift in the presence of strongly relaxing rare earth dopants<sup>32</sup>. Indeed the coupling  $J_c \simeq 120 - 180$  K of the Cu<sup>2+</sup> spins along each of the two (non equivalent<sup>22</sup>) 1D chains of CuGeO<sub>3</sub> is strong enough to ensure a single, exchange-narrowed mode in presence of an antiferromagnetic coupling  $J_N$  (induced on its two Cu<sup>2+</sup> first nearest neighbors) by a Ni<sup>2+</sup>  $S = 1$  spin. In order to account for our observation of a single resonance line, we are forced to assume that (i) either the relaxation rate of the Ni<sup>2+</sup> spin is sufficiently large, compared to  $J_N$ , to decouple the Ni<sup>2+</sup> spins from the precession of the Cu<sup>2+</sup> spins or that (ii) this decoupling occurs through a sufficiently large zero-field splitting removing the Ni<sup>2+</sup> resonance away from the Cu<sup>2+</sup> resonance. In that case, we can modelize the spin dynamics of CuGeO<sub>3</sub>:Ni by two coupled Bloch-like equations, one for the tightly coupled together Cu<sup>2+</sup> spin system (magnetization  $\vec{M}$ ) and one for the fast relaxing Ni<sup>2+</sup> spins (magnetization  $\vec{N}$ ). For sake of simplicity we will assume that the gyromagnetic ratio  $\gamma_{Cu} \simeq \gamma_{Ni} = \gamma$  so that the decoupling occurs only through the relaxation rate of the Ni<sup>2+</sup> spins. The coupled equations are then written with the notation:  $T_{MI}^{-1}$  the Cu spin-lattice relaxation rate,  $T_{NI}^{-1}$  the Ni spin-lattice relaxation rate,  $T_{MN}$  and  $T_{NM}$  the Cu/Ni spin-spin cross relaxation rates between Cu and Ni (related by  $T_{MN}/T_{NM} = N^0/M^0$ , *i.e.* the ratio of the equilibrium magnetizations, by detailed balance<sup>33</sup>).

$$\frac{d\vec{M}}{dt} = \gamma \vec{M} \times (\vec{H} + \lambda \vec{N}) - \frac{\vec{M}}{T_{MN}} + \frac{\vec{N}}{T_{NM}} - \frac{\vec{M} - \vec{M}^0}{T_{MI}} \quad (5)$$

$$\frac{d\vec{N}}{dt} = \gamma \vec{N} \times (\vec{H} + \lambda \vec{M}) - \frac{\vec{N}}{T_{NI}} + \frac{\vec{M}}{T_{MN}} - \frac{\vec{N} - \vec{N}^0}{T_{NI}} \quad (6)$$

Solving for the transverse components as usual leads to the determinant:

$$\begin{vmatrix} \Omega_N & \lambda_N \\ \lambda_M & \Omega_M \end{vmatrix} = 0 \quad (7)$$

with

$$\Omega_M = \omega - \omega_0 - iT_{MI}^{-1} - \lambda_M \quad (8)$$

$$\Omega_N = \omega - \omega_0 - iT_{NI}^{-1} - \lambda_N \quad (9)$$

$$\lambda_M = \gamma \lambda M^0 + iT_{NM}^{-1} \quad (10)$$

$$\lambda_N = \gamma \lambda N^0 + iT_{MN}^{-1} \quad (11)$$

where  $\omega_0$  is the unshifted resonance frequency. In the limit of  $T_{NI}^{-1} \rightarrow \infty$  we get<sup>34</sup>:

$$\omega - \omega_0 = \lambda\gamma N^0 + i(T_{MN}^{-1} + T_{MI}^{-1}) \quad (12)$$

This yields indeed a  $\text{Cu}^{2+}$  resonance shifted to higher fields if  $\lambda < 0$  *i.e.* an antiferromagnetic coupling from  $\text{Ni}^{2+}$  to  $\text{Cu}^{2+}$ , and proportional to the  $\text{Ni}^{2+}$  static magnetization  $N^0$ . However, a major difference appears between our  $\text{CuGeO}_3\text{:Ni}$  model and Kittel's two sublattice model. In the classical sublattice spin dynamics the coupling constant  $\lambda$  represents the exchange energy density, through  $-\lambda\vec{M}_A \cdot \vec{M}_B$ , meaning that every spin A is coupled to every spin B. In our case, we want to specify that the Ni spin is coupled to its two first nearest neighbors  $\text{Cu}^{2+}$  by  $J_N$  and that the effective coupling  $\lambda$  is the resulting average of the Cu-Ni exchange  $J_N$  among the  $\text{Cu}^{2+}$  spins (tightly coupled through  $J_c$ ). This average coupling  $\lambda$  occurs however only from those  $\text{Cu}^{2+}$  spins which are not condensed into singlets  $S = 0$  below the spin Peierls transition. Writing that the exchange energy density is identical in both descriptions yields:

$$\lambda = \frac{2J_N}{\hbar^2\gamma^2} \frac{1}{(1 - n_{SP})\mathcal{N}} \quad (13)$$

where  $n_{SP}$  is the fraction of condensed singlets spins *i.e.* the spin-Peierls order parameter and  $\mathcal{N}$  is the number of Cu ions per unit volume. The shift is then given by:

$$\omega - \omega_0 = \frac{2J_N}{\hbar^2\gamma} \frac{N^0}{(1 - n_{SP})\mathcal{N}} \quad (14)$$

Thus, Eq.(14) indeed predicts the observed dependence for the lineshift (see Eq.(4)). The merit of this formulation is that we use the same argument above and below  $T_{SP}$ . The above equation can be rewritten (in the P phase) in terms of our measured quantities to yield  $J_N$  by:

$$J_N = \frac{1}{2}(g\mu_B)^2 N_A \left[ \frac{\delta B/B_0}{\chi_{Ni}^0} \right] \quad (15)$$

The term between brackets is depicted in the inset of Fig. 10b. We find  $J_N = 75 \pm 10$  K where the error is estimated from the spread of the data at various  $x$  and frequencies. This value for  $J_N$  was checked to be quite consistent with the weak coupling approximation. However this value is three times larger than the one obtained above (§IV) from the fit to the static susceptibility. We think that the value of  $J_N$  derived from the ESR data is closer to the truth since the zero field splitting of the  $\text{Ni}^{2+}$  ion was not incorporated in the susceptibility analysis: This parameter is a priori not required in the ESR model since  $\text{Ni}^{2+}$  is considered as "non resonant".

As concerns the linewidth, a direct application of the weak coupling exchange broadening calculated by Gulley and Jaccarino (equation (2.12) from Ref. 31) with  $J = J_c \simeq 150$  K and  $J' = J_N \simeq 75$  K yields a temperature independent broadening of 8000 G/% Ni, to be compared with 4600 G/% Ni observed between 50 and 300K.

## VI. ANTIFERROMAGNETIC RESONANCE IN Ni-DOPED $\text{CuGeO}_3$

Typical AFMR signals measured in the  $x = 0.04$  sample at 1.8 K in a field applied along the  $a$ ,  $b$ , and  $c$  axes are shown in Fig. 13. Five ESR lines were observed at 21.87 GHz for  $B \parallel a$ . The lines at 0.3, 1.2 and 1.5 T correspond to AFMR lines. The line at 0.75 T originates from a standard DPPH (1,1-diphenyl-2-picrylhydrazyl) sample. The line at 0.7 T probably corresponds to an Electron Paramagnetic Resonance (EPR) signal from the sample. For  $B \parallel b$  and  $B \parallel c$ , one ESR line, which corresponds to an AFMR signal, was observed around 47.5 GHz. The EPR signal which was observed along the  $a$ -axis in the AF ordered state was not observed for these two field directions<sup>35</sup>. This is consistent with the recent theory<sup>36</sup> which predicts the existence of an EPR signal even in the ordered phase when the external field is applied parallel to the easy axis.

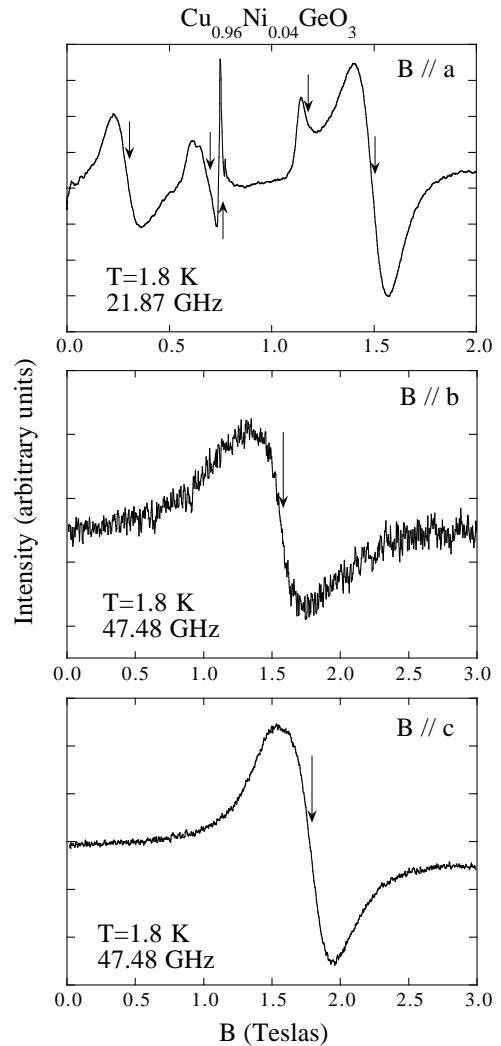


FIG. 13. Typical ESR signals in a single crystal of  $\text{Cu}_{0.96}\text{Ni}_{0.04}\text{GeO}_3$  at 1.8 K for the three crystallographic orientations.

From the AFMR results, we can identify the easy, second-easy, and hard axes as the  $a$ ,  $c$ , and  $b$  axes, respectively, as will be shown below. The angular dependence of the resonance fields at X band was also measured. Resonance points around 0.9 T show a minimum when the field is parallel to the  $a$ -axis. From this result we confirmed that the spins point along the  $a$ -axis within an experimental error of  $\sim 2^\circ$ , which had not clearly been determined by the susceptibility<sup>18</sup> and the neutron scattering measurements<sup>7</sup>. We also performed AFMR measurements in the  $x = 0.03$  sample at  $T = 1.8$  K. The AFMR signals are less clear mainly due to the lower  $T_N$ . However, it was found that the magnetic anisotropy is the same as in the  $x = 0.04$  sample.

Figure 14 shows the frequency vs magnetic-field plot of the resonance points at 1.8 K. Here, the angular frequency ( $\omega$ ) is divided by  $\gamma \equiv 2\pi g\mu_B/h$  ( $\mu_B$ : Bohr magneton,  $h$ : Planck's constant) to express it in magnetic field units and  $B$  is scaled by the  $g$  value for the respective field directions. The  $g$  values we used are,  $g_a = 1.72$ ,  $g_b = 1.80$ , and  $g_c = 1.65$ , which are 80% of the  $g$  values in pure  $\text{CuGeO}_3$  and are also consistent with those obtained from the ESR measurements at  $\sim 5$  K.

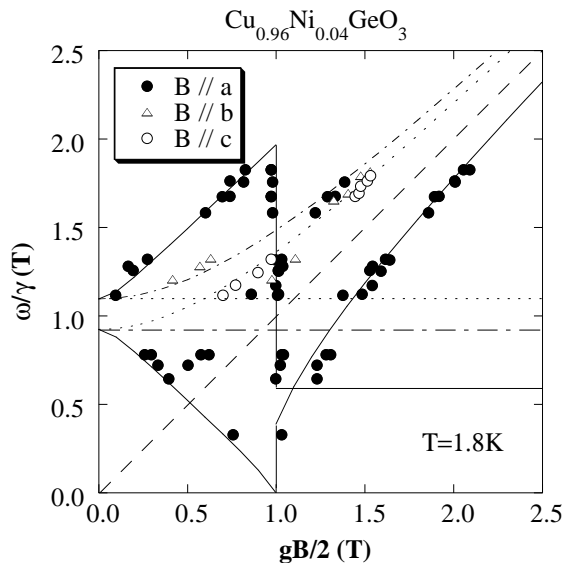


FIG. 14. The frequency vs magnetic-field diagram of the resonance points at 1.8 K in a  $\text{Cu}_{0.96}\text{Ni}_{0.04}\text{GeO}_3$  single crystal. Closed circles, open triangles, and open circles denote experimental data and solid, dash-dotted, and dotted curves are theoretical ones for  $B \parallel a, b$ , and  $c$ , respectively.

TABLE II. Observed  $C_1$ ,  $C_2$ , and  $\alpha$  in  $\text{CuGeO}_3$  doped with Si, Zn, and Ni.

impurity	$T_N$ (K)	$C_1$ ( $\text{T}^2$ )	$C_2$ ( $\text{T}^2$ )	$\alpha$
Si (2%) <sup>a</sup>	4.8	$1.3 \pm 0.1$	$3.8 \pm 0.2$	$0.78 \pm 0.06$
Zn (4%) <sup>b</sup>	4.2	0.89	2.1	0.85
Ni (4%)	4.0	0.85	1.2	0.90

<sup>a</sup>Ref. 17

<sup>b</sup>Ref. 15

The data were analyzed with the AFMR theory for a two-sublattice antiferromagnet with orthorhombic anisotropy<sup>37</sup>. This theory was used in analyzing  $\text{Zn}$ -<sup>15,16</sup> and  $\text{Si}$ -doped samples<sup>17</sup>, and is conveniently reviewed in Ref. 38. We obtained the parameters  $C_1 (=2AK_1) = 0.85$  ( $\text{T}^2$ ),  $C_2 (=2AK_2) = 1.2$  ( $\text{T}^2$ ), and  $\alpha (=1 - \chi_{\parallel}/\chi_{\perp}) = 0.90$ , where  $A$ ,  $K_i$  ( $i = 1$  and  $2$ ),  $\chi_{\parallel}$ , and  $\chi_{\perp}$  are the molecular field coefficient, the anisotropy constants, the susceptibilities along the easy axis and perpendicular to it, respectively. The lines in Fig. 14 are fits with the classical AFMR theory. The parameter  $\alpha$  obtained with AFMR measurements is similar to those in  $\text{Cu}_{0.96}\text{Zn}_{0.04}\text{GeO}_3$ <sup>15,16</sup> and  $\text{CuGe}_{0.98}\text{Si}_{0.02}\text{O}_3$ <sup>17</sup> as shown in Table II but is much larger than that obtained from the magnetic susceptibility measurements ( $\alpha \sim 0.35$ ). The susceptibility parallel to the  $a$ -axis of  $\text{Cu}_{0.96}\text{Ni}_{0.04}\text{GeO}_3$  does not go to zero with decreasing temperature below  $T_N$  as shown in Fig. 2a. This is quite different from what a classical theory of antiferromagnetism predicts for  $\chi_{\parallel}$ . We found that the measured  $\chi_a$  can be interpreted as a sum of a paramagnetic susceptibility which obeys the Curie law and an antiferromagnetic one. The amount of the paramagnetic "centers" is estimated to be about 1% of the total spins assuming  $S = \frac{1}{2}$  and  $g = 2.1$ . The antiferromagnetic susceptibility decreases with decreasing temperature more rapidly than  $\chi_a$ , thus giving a larger value for  $\alpha$ .

We now discuss the origin of the magnetic anisotropy in Ni-doped  $\text{CuGeO}_3$ . In order to explain this, we consider three terms; single ion anisotropy ( $E_{SI}$ ), dipole-dipole ( $E_D$ ), and anisotropic exchange ( $E_{AE}$ ) energies. Moriya and Yosida discussed theoretically the origin of the anisotropy in  $\text{CuCl}_2 \cdot 2\text{H}_2\text{O}$ .<sup>39</sup> They considered both of  $E_D$  and  $E_{AE}$  terms (note that no  $E_{SI}$  term is possible for  $\text{Cu}^{2+}$  spin). They estimated  $|E_D| \sim 10^{-4}$   $\text{cm}^{-1}/\text{ion}$  and  $|E_{AE}| \sim 10^{-3}$   $\text{cm}^{-1}/\text{ion}$ , respectively. Although the crystal structure of  $\text{CuGeO}_3$  is different from that of  $\text{CuCl}_2 \cdot 2\text{H}_2\text{O}$ , we expect that the value of  $E_D$  in  $\text{CuGeO}_3$  is not very much different from the one given above. For  $E_{AE}$  in  $\text{CuGeO}_3$ , we estimate a ten times larger value, because the exchange interaction is about ten times larger than for  $\text{CuCl}_2 \cdot 2\text{H}_2\text{O}$ . On the other hand,  $|E_{SI}| \sim 1$   $\text{cm}^{-1}/\text{ion}$  for  $\text{Ni}^{2+}$  (Ref. 40) so that even a small amount of doping will change drastically the anisotropy of the system. The  $g$  value and the single ion anisotropy constant,  $D$ , for  $\text{Ni}^{2+}$  in an axially distorted octahedral environment are related to the spin-orbit coupling and to the crystal field levels. In the well documented case of trigonal elongation of the octahedron, as in  $\text{CsNiF}_3$ <sup>41</sup>, this distortion leads to  $D > 0$  (and  $g_{\perp}(\text{Ni}) > g_{\parallel}(\text{Ni})$ ). In contrast, in the case of  $\text{CuGeO}_3$ , one expects an elongation to yield  $D < 0$  similar to the Tutton salts<sup>42</sup> and hence give rise to an easy local axis. Here, we denote the single ion anisotropy term as  $DS_z^2$ .

The easy axis for  $\text{Ni}^{2+}$  spin in  $\text{CuGeO}_3$  lies in the  $ab$  plane and is directed alternately when one moves from one site to the other along the  $b$ -axis. Because of the antiferromagnetic interaction, the spins will point either

close to the  $a$ -axis or the  $b$ -axis with antiferromagnetic arrangement along the  $b$ -axis, the former being favoured by  $E_D$ . Thus, the mean easy axis is the  $a$ -axis. Then the easy and second easy axes in Zn- and Si-doped samples are interchanged in the Ni-doped sample.

The  $C_1$  and  $C_2$  values for various impurity-doped  $\text{CuGeO}_3$  are summarized in Table II.  $C_1$  and  $C_2$  correspond to the geometric mean of the exchange field and anisotropy fields along the second-easy and the hard axes, respectively. It is noted that the two parameters are very close in the Ni-doped sample. The parameter  $C_2$  is related to the anisotropy when one rotates the magnetic moments from the  $c$  to  $b$  axes in  $\text{CuGeO}_3\text{:Zn}$  and from the  $a$  to  $b$  axes in  $\text{CuGeO}_3\text{:Ni}$ . In the Zn-doped sample, one loses both of  $E_D$  and  $E_{AE}$  for this rotation, while in the Ni-doped sample,  $E_D$  and a part of  $E_{AE}$  are lost ( $E_{AE}$  in the  $ab$  plane is less anisotropic because  $g_a$  and  $g_b$  are nearly equal). So,  $C_2$  in the Ni-doped sample is smaller than that in the Zn-doped sample. Consequently,  $C_1$  and  $C_2$  become closer in the  $\text{CuGeO}_3\text{:Ni}$  sample.

## VII. CONCLUSION

We have presented in this paper a systematic study of the spin resonance properties of  $\text{CuGeO}_3$  in the paramagnetic, spin-Peierls and antiferromagnetic regimes, when doped with Ni, and compared these new results with previously obtained ESR data on  $\text{CuGeO}_3$  doped with non-magnetic impurities such as Zn, Mg or Si. The main conclusions that we are able to draw are the following:

1- Whereas the investigation of the static susceptibility of doped  $\text{CuGeO}_3$  enables us to define a universal behavior, in the proper reduced units, for the appearance of the paramagnetic, spin-Peierls and antiferromagnetic phases in the Temperature-Concentration diagram, at least two different regimes exist as concern the ESR properties, depending whether the doping atom is magnetic or not.

2- In the case of non-magnetic doping, the resulting  $\text{Cu}^{2+}$  moments responsible for the Curie tail observed below the spin-Peierls temperature  $T_{SP}$  are in strong coupling regime with the spin-Peierls excited triplet, resulting in an unshifted ESR line and a  $c$ -direction easy axis in the AFMR analysis.

3- In presence of doping with  $S = 1 \text{ Ni}^{2+}$ , a weak coupling is found from the analysis of the measured large shift of the  $\text{Cu}^{2+}$  ESR, both in the paramagnetic and the spin-Peierls regimes.

4- However, in order to account for the AFMR  $a$ -easy axis in the latter case, one has to assume that the  $\text{Ni}^{2+}$  ions do participate to the AFMR mode. The origin of the anisotropy in that case is the single ion anisotropy of the  $\text{Ni}^{2+}$  rather than the anisotropic exchange present for pure and (non-magnetic) doped  $\text{CuGeO}_3$ .

5- Although each of these different regimes can be consistently parameterized in a quantitative way, a general description of the dynamics of the transverse spin sus-

ceptibilities of doped spin-Peierls compounds is still an open question.

## VIII. ACKNOWLEDGMENTS

We thank A. K. Hassan for helpful discussions and for the high field EPR of  $\text{CuGeO}_3\text{:Zn}$  single crystals. This work was partially supported by the "MR Science Research Program" from RIKEN. We would like to thank M. Tokunaga for his help in the AFMR measurement. The Institut d'Electronique Fondamentale and Laboratoire de Physico-Chimie de l'Etat Solide are Unités Mixtes de Recherche CNRS: UMR 8622 and UMR 8648, respectively.

---

\* Present address: Advanced Science Research Center, Japan Atomic Energy Research Institute, Tokai, Ibaraki 319-1195, Japan.

\*\* Also at RIKEN Harima Institute, Mikazuki, Sayo, Hyogo 679-5148, Japan.

<sup>1</sup> M. Hase, I. Terasaki, and K. Uchinokura, Phys. Rev. Lett. **70**, 3651 (1993).

<sup>2</sup> J.-P. Pouget, L.-P. Regnault, M. Ain, B. Hennion, J.-P. Renard, P. Veillet, G. Dhalenne, and A. Revcolevschi, Phys. Rev. Lett. **72**, 4037 (1994).

<sup>3</sup> M. Hase, I. Terasaki, Y. Sasago, K. Uchinokura, and H. Obara, Phys. Rev. Lett. **71**, 4059 (1993).

<sup>4</sup> M. Hase, Y. Sasago, K. Uchinokura, G. Kido, and T. Hamamoto, J. Magn. Mater. **140-144**, 1691 (1995).

<sup>5</sup> S. B. Oseroff, S.-W. Cheong, B. Aktas, M. F. Hundley, Z. Fisk, and L. W. Rupp, Jr., Phys. Rev. Lett. **74**, 1450 (1995).

<sup>6</sup> J. G. Lussier, S. Coad, D. F. McMorrow, and D. McK Paul, J. Phys.: Condens. Matter **7**, L325 (1995).

<sup>7</sup> S. Coad, J.-G. Lussier, D. F. McMorrow, and D. McK Paul, J. Phys.: Condens. Matter **8**, 6251 (1996).

<sup>8</sup> T. Masuda, A. Fujioka, Y. Uchiyama, I. Tsukada, and K. Uchinokura, Phys. Rev. Lett. **80**, 4566 (1998).

<sup>9</sup> J.-P. Renard, K. Le Dang, P. Veillet, G. Dhalenne, A. Revcolevschi, and L.-P. Regnault, Europhys. Lett. **30**, 475 (1995).

<sup>10</sup> L.-P. Regnault, J.-P. Renard, G. Dhalenne, and A. Revcolevschi, Europhys. Lett. **32**, 579 (1995).

<sup>11</sup> Y. Sasago, N. Koide, K. Uchinokura, M. C. Martin, M. Hase, K. Hirota, and G. Shirane, Phys. Rev. B **54**, R6835 (1996).

<sup>12</sup> H. Fukuyama, T. Tanimoto, and M. Saito, J. Phys. Soc. Jpn. **65**, 1182 (1996).

<sup>13</sup> B. Grenier, J.-P. Renard, P. Veillet, C. Paulsen, G. Dhalenne, and A. Revcolevschi, Phys. Rev. B **58**, 8202 (1998).

- <sup>14</sup> M. Hase, K. Uchinokura, R. J. Birgeneau, K. Hirota, and G. Shirane, *J. Phys. Soc. Jpn.* **65**, 1392 (1996).
- <sup>15</sup> M. Hase, M. Hagiwara, and K. Katsumata, *Phys. Rev. B* **54**, R3722 (1996).
- <sup>16</sup> P. Fronzes, M. Poirier, A. Revcolevschi, and G. Dhahlenne, *Phys. Rev. B* **56**, 7827 (1997).
- <sup>17</sup> H. Nojiri, T. Hamamoto, Z. J. Wang, S. Mitsudo, M. Motokawa, S. Kimura, H. Ohta, A. Ogiwara, O. Fujita, and J. Akimitsu, *J. Phys.: Condens. Matter* **9**, 1331 (1997).
- <sup>18</sup> N. Koide, Y. Sasago, T. Masuda, and K. Uchinokura, *Czechoslovak J. Phys.* **46**, 1981 (1996).
- <sup>19</sup> S. Oseroff, S-W. Cheong, A. Fondado, B. Aktas, and Z. Fisk, *J. Appl. Phys.* **75**, 6819 (1994).
- <sup>20</sup> I. Yamada, M. Nishi, and J. Akimitsu, *J. Phys.: Condens. Matter* **8**, 2625 (1996).
- <sup>21</sup> M. Honda, T. Shibata, K. Kindo, S. Sugai, T. Takeuchi, and H. Hori, *J. Phys. Soc. Jpn.* **65**, 691 (1996).
- <sup>22</sup> B. Pilawa, *J. Phys.: Condens. Matter* **9**, 3779 (1997).
- <sup>23</sup> M. Hase, *J. Magn. Magn. Mater.* **177-181**, 611 (1998).
- <sup>24</sup> A. K. Hassan, L. A. Pardi, G. B. Martins, G. Cao, and L.-C. Brunel, *Phys. Rev. Lett.* **80**, 1984 (1998).
- <sup>25</sup> V. N. Glazkov, A. I. Smirnov, O. A. Petrenko, D. M. K. Paul, A. G. Vetkin, and R. M. Eremina, *J. Phys.: Cond. Mat.* **10**, 7879 (1998).
- <sup>26</sup> B. Grenier, J.-P. Renard, P. Veillet, C. Paulsen, R. Calmeczuk, G. Dhahlenne, and A. Revcolevschi, *Phys. Rev. B* **57**, 3444 (1998).
- <sup>27</sup> Among the twelve investigated samples (doped with 1.6, 3.9 and 10% Zn, 1, 3 and 5% Mg, 0.2, 0.7, 0.85, 1.5, 6 and 8.5% Si), the linewidth was found to be always the same as in pure CuGeO<sub>3</sub> except for the 0.7% Si- and 3.9% Zn-doped samples, where a temperature independent constant broadening (of  $\simeq 200$  Gauss along  $a$  and  $c$ ,  $\simeq 400$  G along  $b$ ) was measured.
- <sup>28</sup> M. Hase, N. Koide, K. Manabe, Y. Sasago, K. Uchinokura, and A. Sawa, *Physica B* **215**, 164 (1995).
- <sup>29</sup> B. Grenier and P. Monod, to be published.
- <sup>30</sup> Note that the results from the 0.2% Ni-doped sample and the pure one can be directly compared on the same  $T$  scale since the spin-Peierls temperatures are very close to each other (see Table I).
- <sup>31</sup> J. E. Gulley and V. Jaccarino, *Phys. Rev. B* **6**, 58 (1972).
- <sup>32</sup> C. Kittel, *Phys. Rev.* **115**, 1587 (1959).
- <sup>33</sup> S. E. Barnes, *Adv. Phys.* **30**, 801 (1981).
- <sup>34</sup> In Kittel's paper, due to the particular form of the damping specific to ferrimagnetic materials, a special case of strong coupling in presence of infinite relaxation rate is obtained. This results in a shift which is independent from the coupling contrary to Eq. (12) of the present work. The latter is simply related to the "unbottleneck" situation.
- <sup>35</sup> This fact shows that this EPR line cannot be attributed to free Cu spins (see for instance M. Hagiwara, K. Katsumata, I. Yamada, and H. Suzuki, *J. Phys.: Condens. Matter* **8**, 7349 (1996)). However, we note that the 0.5 T linewidth of the 3.2% Ni sample used by Glazkov et al. (Ref. 25 Fig. 3) precludes a detailed comparison with the present results obtained on high quality samples (0.2 T linewidth).
- <sup>36</sup> A. Ogasahara and S. Miyashita, *J. Phys. Soc. Jpn* **69**, 4043 (2000).
- <sup>37</sup> T. Nagamiya, K. Yosida, and R. Kubo, *Adv. Phys.* **4**, 1 (1955).
- <sup>38</sup> K. Katsumata, *J. Phys.: Condens. Matter* **12**, R589 (2000).
- <sup>39</sup> T. Moriya and K. Yosida, *Prog. Theor. Phys.* **9**, 663 (1953).
- <sup>40</sup> A. Abragam, B. Bleaney "Electron paramagnetic resonance of transition ions", Clarendon Press. Oxford, p. 450 (1970).
- <sup>41</sup> see for instance, C. Dupas and J.-P. Renard, *J. Phys. C: Solid State Phys.* **10**, 5057 (1977).
- <sup>42</sup> J. H. E. Griffiths and J. Owen, *Proc. Roy. Soc. A* **213**, 459 (1952).